Spatial Distribution of Added Homopolymer within the Microdomains of a Mixture Consisting of an ABA-Type Triblock Copolymer and a Homopolymer

Kohtaro Kimishima and Takeji Hashimoto*

Division of Polymer Chemistry, Graduate School of Engineering, Kyoto University, Kyoto 606, Japan

Chang Dae Han

Department of Polymer Engineering, The University of Akron, Akron, Ohio 44325-0301

Received December 9, 1994; Revised Manuscript Received March 13, 1995[⊗]

ABSTRACT: The ordered structure was investigated in binary mixtures of an ABA-type triblock copolymer and a homopolymer. For the study, we employed (a) binary mixtures of polystyrene-*block*-polybutadiene-*block*-polystyrene copolymer (Kraton D-1102, Shell Development Co.) (hereafter abbreviated as K1102) and homopolymer poly(α-methylstyrene) (PαMS4) having the number-average molecular weight (M_n) of 3200 and (b) binary mixtures of K1102 and homopolymer polystyrene (PS4) having M_n of 2800. Emphasis was placed on the effect of the chemical structure of added homopolymer on the spatial distribution within the microdomains of the mixtures. The morphology of the mixtures was investigated as a function of the volume fraction of added homopolymer (PαMS4 or PS4) and temperature by small-angle X-ray scattering (SAXS) and transmission electron microscopy (TEM). The SAXS profiles obtained were analyzed by using one-dimensional paracrystal analysis. It was found that added homopolymer, PαMS4 or PS4, was solubilized in the PS microdomains of K1102 but the spatial distribution of the added homopolymer within the PS microdomains was different. Specifically, both the results of TEM and SAXS indicate that the added PαMS4 was *not* distributed uniformly within the PS microdomains of K1102, showing a tendency of being *localized* at the center of the PS microdomains, whereas the added PS4 was distributed *uniformly* within the PS microdomains of K1102. The localization observed in the K1102/PαMS4 mixtures was ascribed to the repulsive interaction between the PS chains in K1102 and added homopolymer PαMS chains. However, we observed a tendency that added PαMS was distributed *uniformly* within the PS microdomains of K1102 as the temperature was raised. This was explained by the temeperture dependence of the interaction parameter between PS and PαMS.

I. Introduction

In recent years, numerous experimental studies have been reported on the morphology,[1–14] phase equilibria,[11,15,16] and order–disorder transition[3,11,15–19] in binary mixtures of a block copolymer and a homopolymer. When a homopolymer is added to a block copolymer, one must distinguish two situations: one is the situation where added homopolymer has the same chemical structure as one of the constituent components of the block copolymer[1–10,15–19] (e.g., a situation where a homopolymer PS is added to a polystyrene-*block*-polyisoprene (SI diblock) or polystyrene-*block*-polybutadiene (SB diblock) copolymer) and the other is the situation where added homopolymer has a different chemical structure from that of either of the constituent components of the block copolymer.[11–14] This distinction is very important from the point of view of understanding the spatial distribution of added homopolymer within the microdomains of the block copolymer. In order to facilitate our presentation below, we shall use the following convention: (a) (A-*block*-B)/A or (A-*block*-B)/B mixture when homopolymer A or homopolymer B is added to a block copolymer A-*block*-B, and (b) (A-*block*-B)/C mixture when homopolymer C is added to a block copolymer A-*block*-B.

Mixtures consisting of a block copolymer and a homopolymer can have a variety of microdomain structures, depending upon (i) the molecular weight of added homopolymer relative to the molecular weight of the block copolymer, (ii) the concentration of added homopolymer in the mixture, (iii) block copolymer composition, and (iv) temperature. To make the matter more complicated, there are two types of phase transition that one encounters when a homopolymer is added to a block copolymer,[20,21] namely (a) *microphase transition* which is induced by the block copolymer itself, and (b) *macrophase transition* in which the excess amount of added homopolymer forms a separate phase. Using the random phase approximation,[22] we can estimate the stability limits[21,23] and construct phase diagrams for (A-*block*-B)/A, (A-*block*-B)/B, or (A-*block*-B)/C mixtures[24,25] for microphase and macrophase transitions.

Using small-angle X-ray scattering (SAXS) and transmission electron microscopy (TEM), Hashimoto and coworkers[1,2,26,27] investigated the ordered structure of SI diblock copolymer/homopolymer PS mixtures and discussed the dependence of the molecular weight of added homopolymer PS on the spatial distribution within the PS microdomains of the SI diblock copolymer. The spatial distribution of the homopolymer PS within the PS microdomains was further studied by a combined SAXS and small-angle neutron scattering (SANS) for the dry brush criterion,[28] which directly confirmed the earlier results.[1] Using neutron reflectivity, Mayes et al.[29] investigated the spatial distribution of added homopolymer polystyrene (PS) or homopolymer poly(methyl methacrylate) (PMMA) within the microdomains of PS-*block*-PMMA copolymer in the spin-coated thin films. They found that (1) when the molecular weight of added PMMA was comparable to that of the corresponding copolymer block, it was *not* distributed uniformly within the PMMA microdomains,

[⊗] Abstract published in *Advance ACS Abstracts,* April 15, 1995.

0024-9297/95/2228-3842$09.00/0 © 1995 American Chemical Society

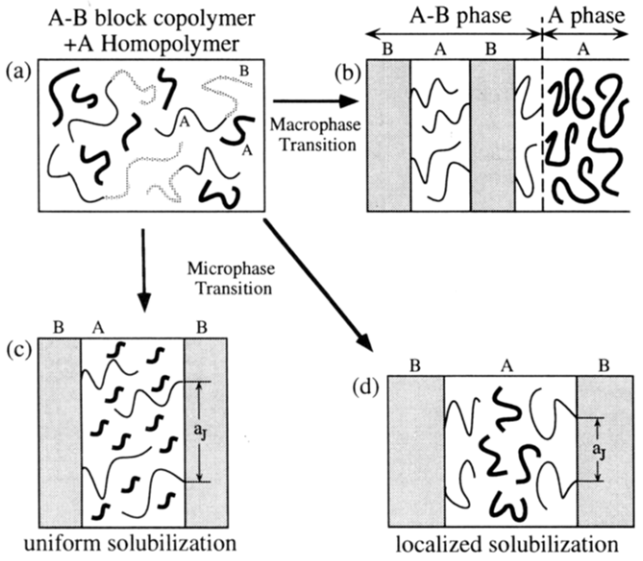

Figure 1. Schematic describing the spatial distribution of added homopolymer A in (a) the case of a homogeneous mixture of A–B and A, (b) the case of the macrophase separation between A–B and A, and the case where A is solubilized uniformly in A microdomains (c) and nonuniformly in the middle of A microdomains (d).

localizing at the center of the microdomains, and (2) as the molecular weight of added PMMA was decreased, it was distributed more *uniformly* within the PMMA microdomains of the PS-*block*-PMMA copolymer. Such experimental observations were found to be in agreement with theoretical prediction[30] and consistent with results reported for bulk film specimens.[1,2,28]

Figure 1 shows a schematic describing possible ordered structures of an (A-*block*-B)/A mixture. When macrophase transition occurs in the mixture, the chains of homopolymer A separate from the chains of the A-*block*-B copolymer and form *macroscopic* domains of A (i.e., (a) → (b) in Figure 1). However, when the entire amount of added homopolymer A is solubilized in the microdomains of the A-*block*-B copolymer, two extreme situations may be considered: (i) the chains of homopolymer A are mixed on the molecular level with the chains of block A of the A-*block*-B copolymer (i.e., *uniform* solubilization as indicated by (a) → (c) in Figure 1), and (ii) the chains of homopolymer A are *not* uniformly mixed with the chains of block A of the A-*block*-B copolymer and tend to localize at the center of the microdomains (i.e., *localized* solubilization, as indicated by (a) → (d) in Figure 1).

The thermodynamic factors which affect the extent of solubilization of homopolymer A in the microdomains of the A-*block*-B copolymer are (1) the contact energy (E_{inter}) between different components A and B at the interface, (2) the combinatorial entropy (ΔS_{comb}) between the chains of the block copolymer and the chains of the homopolymer, and (3) the conformational entropy (ΔS_{conf}) of the chains of the block copolymer and of the homopolymer. When the chains of homopolymer A are uniformly solubilized in the A microdoamins of the A-*block*-B copolymer and the A microdoamins swell, the average distance between the neighboring chemical junctions (a_J) of the block copolymer is increased and the interfacial area per single block chain is increased. This will then increase E_{inter}. The *localized* solubilization of homopolymer A is favorable to E_{inter}. Block copolymer chains in the microdomain structure are stretched in the direction perpendicular to the interface,[31–33] and the chains of homopolymer A which are solubilized uniformly in the lamellae are also stretched in the same direction.[34] The stretched polymer chains lose their conformational entropy and thus ΔS_{conf} prefers localized solubilization of homopolymer A, because the degree of chain stretching is expected to be less, as compared to the situation where uniform solubilization takes place. On the other hand, ΔS_{comb} obviously has an advantage in the case of uniform solubilization of homopolymer A in the A microdomains. The manner of solubilization of homopolymer A in the A microdomains of the A-*block*-B copolymer is determined by the balances among these three factors, E_{inter}, ΔS_{conf}, and ΔS_{comb}, such that the free energy of the system can be minimized. When the molecular weight (M_{homo}) of homopolymer A increases, the contribution of ΔS_{comb} to the free energy decreases, because ΔS_{comb} is related to the inverse of degree of polymerization (N) of the homopolymer. Thus the added homopolymer A tends to be localized at the center of the microdomains of the block copolymer A-*block*-B or forms separate *macroscopic* domains.

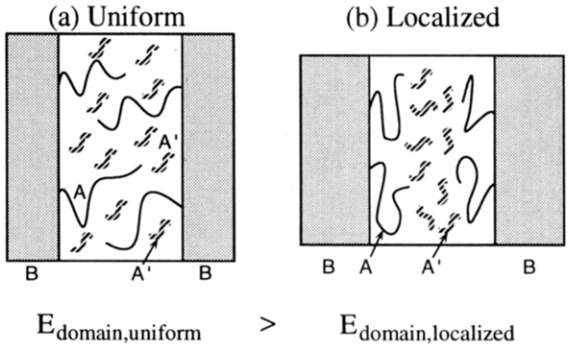

Figure 2. Schematic describing the spatial distribution of added homopolymer A′ within the microdomains of the block copolymer A-*block*-B, where block chains A and B are assumed to form microdomains A and B, respectively. A′ is assumed to be selectively solubilized into A microdomains. (a) Uniform and (b) localized solubilization of A′ into A microdomains. B block chains in the B microdomains are not drawn in the diagram.

The above observation can be extended to a situation where a homopolymer C is added to an A-*block*-B copolymer, in which the chemical structure of C is different from that of either block A or block B. If added homopolymer C has *no* chemical affinity with either block A or block B, it will then form a separate macroscopic phase. However, when added homopolymer C has a chemical affinity with one of the blocks which forms microdomains, it will then have a possibility to be solubilized in one of the microdomains of the A-*block*-B copolymer. Let us now assume that added homopolymer C has a chemical affinity with block A (forming microdomains) of an A-*block*-B copolymer. For convenience, let us designate the added homopolymer with the notation A′, in order to indicate that it has a greater chemical affinity with block A than with block B. For (A-*block*-B)/A′ mixtures, we must consider an additional factor, the contact energy (E_{domain}) between the component A and component A′ within the microdomain, in order to describe the extent of solubilization of added homopolymer A′ in the A microdomains, where we assume that block A forms microdomains. Figure 2 gives a schematic describing possible ordered structures of the (A-*block*-B)/A′ mixture in which A′ is solubilized in A microdomains, namely, (a) *uniform* solubilization and (b) *localized* solubilization. When the interaction

Table 1. Molecular Characteristics of the Polymers Employed

sample code	M_n	M_w/M_n	PS (wt %)	density (g/cm^3) at 30 °C
K1102	6.16×10^4 [a]	1.21[b]	28[c]	$\varrho_{K1102} = 0.94$[c] $\varrho_{PS} = 1.07$[d] $\varrho_{PB} = 0.899$[e]
PαMS4	3.2×10^3 [b]	1.3[b]	0	1.13[f]
PS4	2.8×10^3 [c]	1.05[c]	100	1.06[d]

[a] Determined by membrane osmometry. [b] Determined by gel permeation chromatography. [c] Supplied by the manufacturer. [d] Calculated using the following expression:[35] $1/\varrho_{PS} = 0.9199 + 5.098 \times 10^{-4}(T - 273) + 2.354 \times 10^{-7}(T - 273)^2 + (32.46 + 0.1017(T - 273))/M_{w,PS}$, where T is the absolute temperature and $M_{w,PS}$ is the molecular weight of PS. [e] Calculated from ϱ_{K1102}, ϱ_{PS}, and the weight fraction of PS block. [f] Calculated using the following expression:[36] $1/\varrho_{P\alpha MS} = 0.87 + 5.08 \times 10^{-4}(T - 273)$, where T is the absolute temperature.

between the components A and A′ is repulsive, the added homopolymer A′ tends to be localized at the center of the microdomains A (part b). However, it can be easily surmised that the extent of localization of added homopolymer A′ in an (A-*block*-B)/A′ mixture would be different from that of added homopolymer A in an (A-*block*-B)/A mixture. This is the subject dealt with in this paper. The above discussion on A-*block*-B/A′ should be further extended to mixtures of A-*block*-B-*block*-A/A′ in our problem where the A-*block*-B is replaced by an A-*block*-B-*block*-A. The replacement would certainly affect the various physical factors discussed above, because both chain ends of B blocks are linked to A blocks and are localized at interfaces between the A and B microdomains, forming either bridge or loop configurations. Although a comparison of the behaviors of A−B−A/A′ and A−B/A′ is an interesting theme to be explored, we will not focus on this problem in this work.

II. Experimental Section

A. Materials. In this study, we employed a polystyrene-*block*-polybutadiene-*block*-polystyrene (SBS triblock) copolymer (Kraton D-1102, Shell Development Co.), which, for brevity, will hereafter be designated as K1102, and two homopolymers: (i) poly(α-methylstyrene) (PαMS4) having the number-average molecular weight (M_n) of 3200, which was synthesized via anionic polymerization in our laboratory, and (ii) polystyrene (PS4) having $M_n = 2800$, which was supplied by Tosoh Co., Ltd., in Japan. Table 1 gives a summary of the molecular characteristics of the materials.

Samples were prepared by the solvent-casting method. Predetermined amounts of K1102 and homopolymer (PαMS4 or PS4) were dissolved in toluene (ca. 5 wt % solution). The solvent was evaporated slowly for 10 days at 30 °C and dried under vacuum for 3 days until no weight loss was observed. Then the samples were annealed at 150 °C under vaccuum for 2 h. The thickness of the prepared specimen was about 0.5 mm.

B. Small-Angle X-ray Scattering (SAXS). SAXS measurements were conducted with an apparatus consisting of a 12 kW rotating-anode X-ray generator, a graphite crystal for the incident beam monochromatization, a 1.5 m camera, and a one-dimensional position-sensitive proportional counter. Cu Kα radiation with a wavelength of 0.1542 nm was used. SAXS profiles were corrected for absorption, air scattering, sample thickness, slit-height and slit-width smearings, and the thermal diffuse scattering arising from density fluctuations.

SAXS profiles were measured as a function of volume fraction of added homopolymer and temperature. Typical measurement time for one specimen was about 3 h at a given temperature, but it was about 1 h when the temperatures were higher than 100 °C. All SAXS profiles reported in this paper were measured at through-view in which the X-ray incident beam was perpendicular to the film surface.

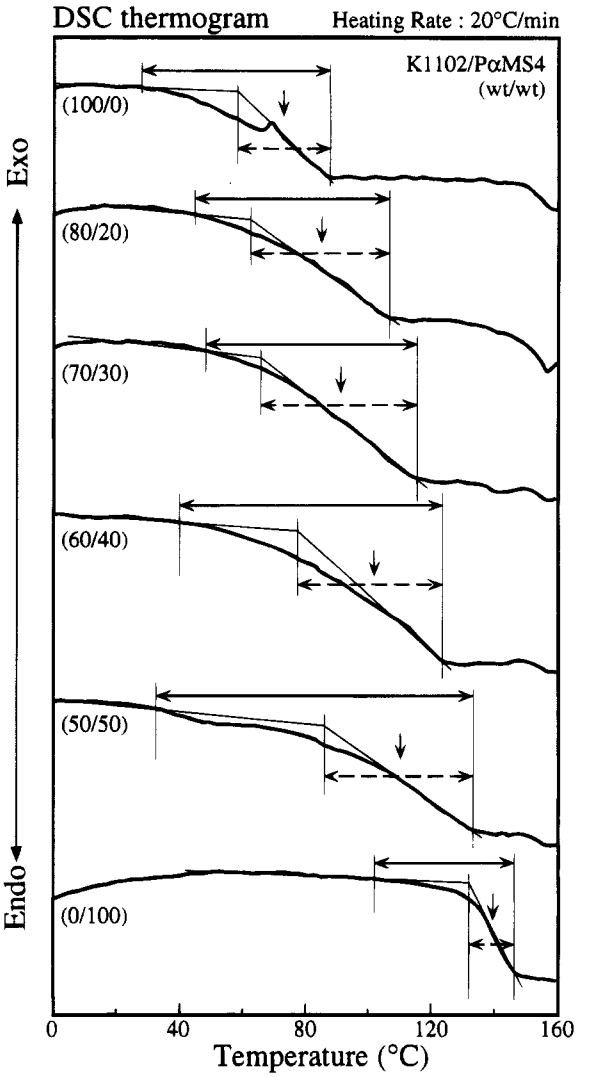

Figure 3. DSC thermograms for the K1102/PαMS4 mixtures, where the vertical arrows indicate the glass transition temperature at the midpoint and the horizontal arrows indicate the breadth of the transition.

C. Transmission Electron Microscopy (TEM). A small piece of film specimen was stained by osmium tetraoxide vapor, and the stained specimen was embedded in epoxy resin. The stained and embedded specimen was microtomed to ultrathin sections of 50−90 nm in thickness using a Reichert Ultracut E at about −100 °C. The ultrathin sections thus obtained were stained by osmium tetraoxide vapor for about 4 h. Then the microdomain structure in the ultrathin section was observed using a transmission electron microscope (Hitachi H-600).

D. Differential Scanning Calorimetry (DSC). DSC measurements were conducted with the Perkin-Elmer DSC System 7. The weight of the specimen was about 15 mg for mixtures of block copolymer and homopolymer and 5 mg for homopolymer. First, a specimen was heated at a rate of 20 °C/min from −30 to +185 °C, held at 185 °C for 30 s, and quenched quickly to −30 °C and then a second scan was made at the same heating rate and temperature range. We found that the DSC thermogram obtained in the first scan was almost identical to that obtained in the second scan.

III. Results

A. DSC Measurement. Figure 3 gives DSC thermograms for block copolymer K1102, homopolymer PαMS4, and their mixtures. It can be seen in Figure 3

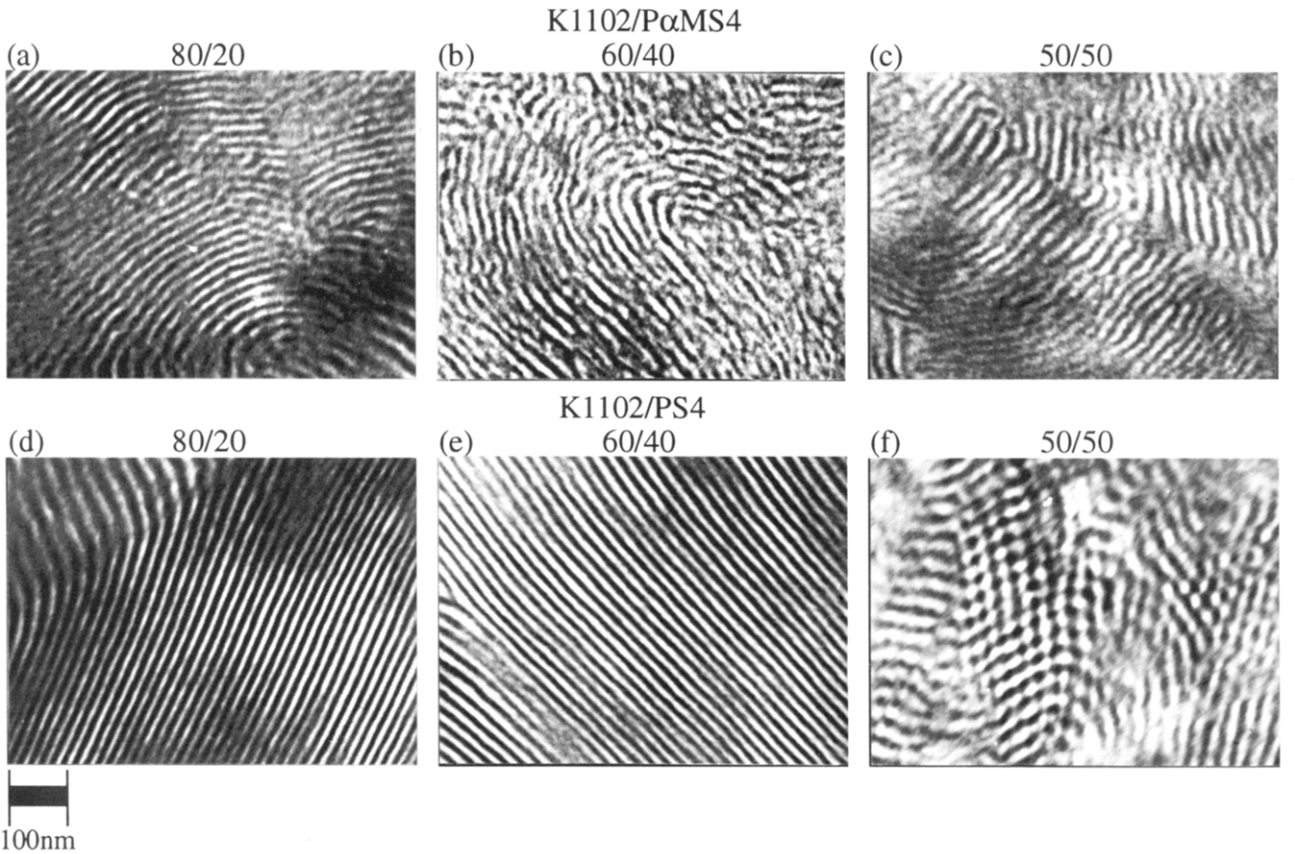

Figure 4. Transmission electron micrographs for (a) 80/20 K1102/PαMS4, (b) 60/40 K1102/PαMS4, (c) 50/50 K1102/PαMS4, (d) 80/20 K1102/PS4, (e) 60/40 K1102/PS4, and (f) 50/50 K1102/PS4.

Table 2. Summary of the Glass Transition Temperatures of the K1102/PαMS4 Mixtures

width of glass transition ΔT_g (°C)	blend composition (by weight percent)					
	100/00	80/20	70/30	60/40	50/50	00/100
from horizontal solid-line arrow	60	63	69	85	101	44
from horizontal dashed-line arrow	30	45	50	47	47	13
glass transition T_g (°C)[a]	73	84	91	102	110	139

[a] Determined from the positions shown by the vertical arrows in Figure 3.

that only one glass transition temperature (T_g) exists over the temperature range covered and over the entire range of blend compositions investigated and the T_g of the mixture increases with increasing amount of PαMS4, suggesting that added PαMS4 was solubilized in the PS microdomains of K1102. It is of interest to observe in Figure 3 that the glass transition of the K1102/PαMS4 mixture is very broad, as compared to that of the PS block of K1102 and that of homopolymer PαMS4, and that the width of the glass transition increases with increasing amount of PαMS4 up to 50 wt %. The width of the glass transition is summarized in Table 2. The broadness of the glass transition, observed in Figure 3, for the K1102/PαMS4 mixtures suggests that added PαMS4 was *not* uniformly distributed within the PS microdomains of K1102. Below we will elaborate on this further when presenting the results of SAXS and TEM measurements.

B. TEM Observation. Figure 4 shows transmission electron micrographs of K1102/PαMS4 mixtures (Figures 4a–c) and K1102/PS4 mixtures (Figures 4d–f), in which the dark areas represent the polybutadiene (PB) phase stained by osmium tetraoxide and the bright areas represent the PS4 and PαMS4 phases. It should be mentioned that K1102 has cylindrical microdomains of PS, as reported in our previous paper.[11] The following observations are worth noting in Figure 4. (1) Both the 80/20 K1102/PαMS4 and the 80/20 K1102/PS4 mixtures form a lamellar microdomain structure but the regularity of the microdomains is much greater in the 80/20 K1102/PS4 mixture than in the 80/20 K1102/PαMS4 mixture. (2) As the amount of added homopolymer was increased from 20 to 40 wt %, both the 60/40 K1102/PαMS4 and the 60/40 K1102/PS4 mixtures still have lamellar microdomains. Notice, however, that the regularity of microdomains was poorer in the 60/40 K1102/PαMS4 mixture as compared to that in the 80/20 K1102/PαMS4 mixture, whereas the regularity of the microdomains in the K1102/PS4 mixtures was *not* affected as the amount of added PS4 was increased from 20 to 40 wt %. In other words, the interface between the two lamellae (i.e., PB lamellae and PS/PαMS lamellae) in the 60/40 K1102/PαMS4 mixture is *wavy* and the regularity of the microdomains is rather poor. On the other hand, both the 80/20 K1102/PS4 and the 60/40 K1102/PS4 mixtures have straight interfaces, indicating higher long-range order. (3) As the amount of added homopolymer was increased further to 50 wt %, we observe a dramatic difference in the microdomain structure between the 50/50 K1102/PS4 mixture and the 50/50 K1102/PαMS4 mixture. Specifically, the 50/50 K1102/PS4 mixture has PB cylindrical microdomains in a PS matrix, indicating that a morphological transition from lamellae to cylinders took place as the amount of added homopolymer PS increased from 40 to 50 wt % (see Figures 4e and 4f). However, *no* morphological transition took place as the amount of PαMS4 was

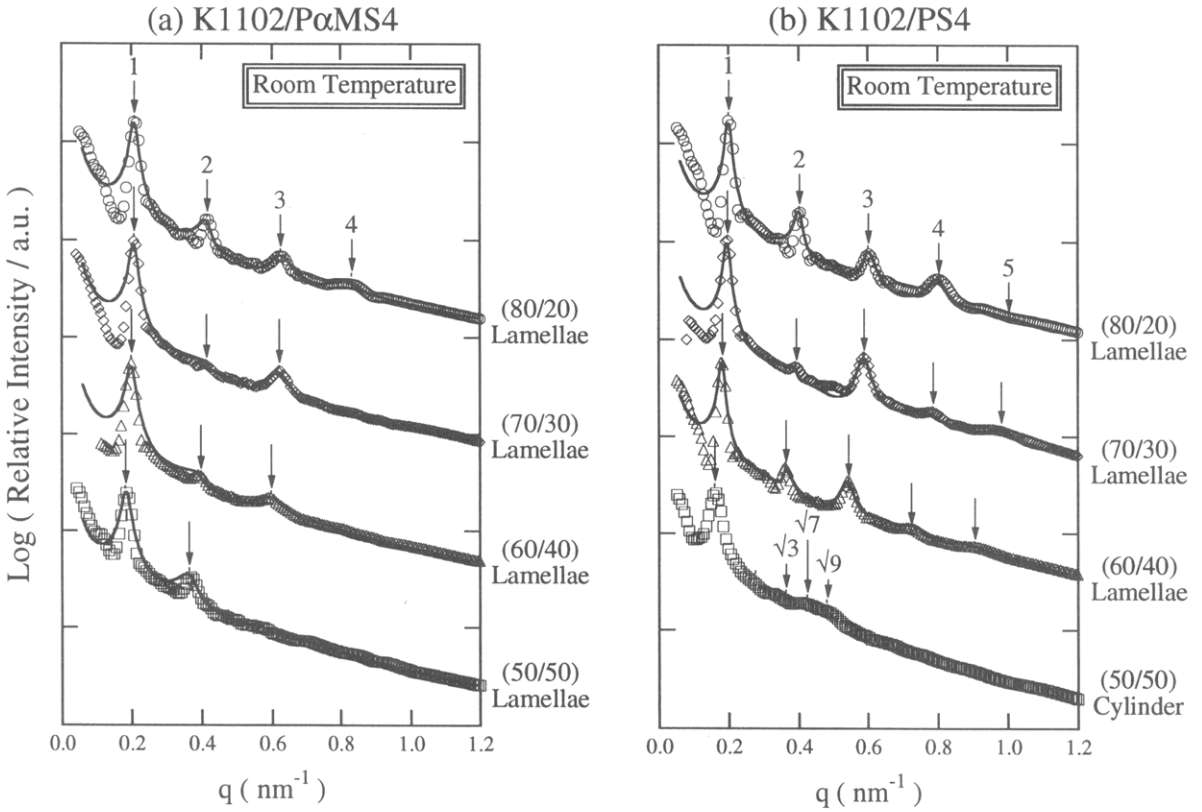

Figure 5. Plot of relative scattering intensity versus wave vector q, taken at room temperature, for (a) K1102/PαMS4 mixtures and (b) K1102/PS4 mixtures, where different symbols denote different blend compositions. The solid lines denote the best-fit curves calculated using one-dimensional paracrystal theory.

increased from 40 to 50 wt % in the K1102/PαMS4 mixtures. This difference is attributable to the way in which added homopolymer (PS4 or PαMS4) was distributed within the microdomains of K1102. Below we will elaborate further on this after presenting SAXS results.

C. SAXS Measurement. Figure 5 gives SAXS profiles taken at room temperature for (a) the K1102/PαMS4 mixtures and (b) the K1102/PS4 mixtures. The solid lines in Figure 5 are best-fit curves, which were calculated using one-dimensional paracrystal theory, the details of which will be discussed below. It should be mentioned that SAXS profiles for *neat* block copolymer K1102 were reported in our previous paper.[11] The following observations are worth noting in Figure 5. (1) Both K1102/PαMS4 and K1102/PS4 mixtures with the compositions of 80/20, 70/30, and 60/40 have a lamellar microdomain structure, judging from the positions of higher order scattering maxima at the scattering vectors q of multiple integers relative to the position of the first-order scattering maximum. This suggests that when PαMS4 or PS4 was added to K1102, it was solubilized in the PS microdomains of K1102 and changed the curvature of the interface. As a result, the microdoamin structure changed from cylinders composed of PS block chains in the matrix of PB chains to alternating lamellae composed of PB and PS chains solublized with added PαMS4 or PS4. (2) The 50/50 K1102/PS4 mixture has cylindrical microdomains of PB, judging from the positions of higher order scattering maxima at the scattering vectors q of 1, $\sqrt{3}$, $\sqrt{7}$, and $\sqrt{9}$ relative to the position of the first-order scattering maximum. However, the 50/50 K1102/PαMS4 mixture has lamellar microdomains having alternating layers of PB and PS solubilized with added PαMS4. (3) The higher order scattering maxima are observed more clearly in the K1102/PS4 mixtures than in the K1102/PαMS4 mixtures, indicating that the long-range order of the lamellar microdomains is greater in the K1102/PS4 mixtures than in the K1102/PαMS4 mixtures. These observations made from the SAXS profiles are in complete agreement with those made above from TEM.

Figure 6 gives typical SAXS profiles taken *in situ* at various temperatures for (a) the 70/30 K1102/PαMS4 mixture and (b) the 70/30 K1102/PS4 mixture. It can be seen in Figure 6 that the higher order scattering maxima disappear with increasing temperature, and at high temperatures the SAXS profiles show only broad first-order peaks. The scattering vector q of the first-order scattering maximum increased with increasing temperature, and at high temperatures the value of $q = q_m$ at which the first-order scattering maximum occurs becomes independent of temprature. The details of the temperature dependence of q_m will be discussed in the next section.

IV. Discussion

A. Spatial Distribution of Added Homopolymer Observed from TEM. How can we qualitatively interpret the extent of regularity of the microdomain structure formed by the mixtures of block copolymer K1102 and homopolymer PS4 or PαMS4 as observed by TEM in section IIIB? It should be related to the spatial distribution of added homopolymer within the PS microdomains of K1102. In order to facilitate our discussion here, let us refer to the schematic given in Figure 7. When added PαMS4 is *not* distributed uniformly within the microdomain in the direction *perpendicular* to the interface (see Figure 7a), the interaction between block chains (the chains indicated by the arrows in Figure 7a) that belong to the opposing interfaces was

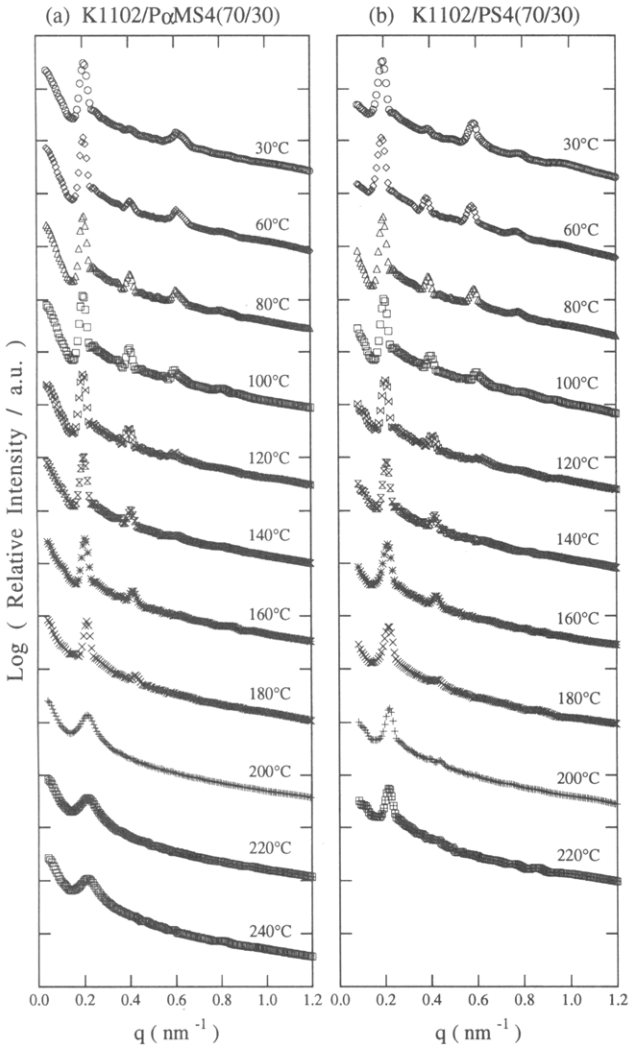

Figure 6. Plots of relative scattering intensity versus wave vector q, taken at various temperatures indicated, for the (a) K1102/PαMS4 (70/30) and (b) K1102/PS4 (70/30) mixtures.

screened. This makes the interface undulated at a length scale greater than the persistence length of the lamellae[26] (locally the interface is flat), so that the long-range order of microdomains decreased.

Figure 7b depicts schematically the situation where added PαMS4 is *not* distributed uniformly within the microdomains in the direction *parallel* to the interface. In such a situation, within the microdomains composed of PS block and added PαMS4 one finds that the concentration of PαMS4 is greater in one region than in other regions. The interface between PB microdomains and the microdomains composed of PS block and PαMS4 passing through such two regions has a curvature and consequently the interfacial area is increased. The free energy will be increased owing to the loss of the combinatorial entropy of PαMS4 and the increase in the interfacial area. On the other hand, the free energy will be decreased owing to the reduction of the interaction energy betwen the PαMS4 and the PS within the microdomains. The balance of these two opposing physical factors will determine the spatial distribution of PαMS4 in the PS microdomains of K1102.

On the basis of the argument presented above, we can conclude that the lower degree of regularity observed in the lamellar microdomains of K1102/PαMS4 mixtures signifies *nonuniform* distributions of added homopolymer PαMS4 in the direction *perpendicular* to the

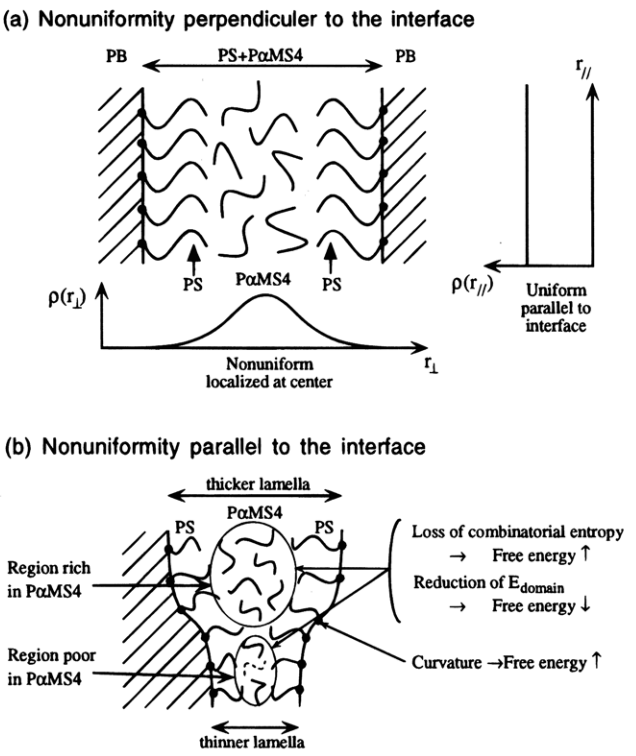

Figure 7. Schematic describing the spatial distribution of added homopolymer PαMS4 within the PS microdomains of the block copolymer K1102: (a) nonuniform distribution perpendicular but uniform distribution parallel to the interface, giving rise to a flat interface; (b) nonuniform distribution both parallel and perpendicular to the interface, giving rise to a wavy interface. $\varrho(r_{\parallel})$ and $\varrho(r_{\perp})$ show the spatial distribution of PαMS4 parallel and perpendicular to the interface, respectively. The shaded and unshaded phases correspond to the PB microdomains and the microdomains composed of PS block chains and PαMS4 homopolymers.

interface (see Figure 7a) as well as *parallel* to the interface (see Figure 7b).

B. Spatial Distribution of Added Homopolymer Observed from SAXS Measurement. In order to discuss the microdomain structure of the K1102/PαMS4 and K1102/PS4 mixtures, respectively, from SAXS measurements, we applied one-dimensional paracrystal analysis to the SAXS profiles.

(a) Paracrystal Analysis. Let us consider the schematic given in Figure 8, where (i) the lamellar microdomain structure is represented by an assembly of the grain units with a certain orientation (see Figure 8a), (ii) one grain unit consists of the alternating disk-like particles A and B with the thicknesses L_A and L_B, respectively, and the diameter ξ, which is the persistence length of the lamellae along the interface (see Figure 8b), and (iii) the electron density profile $\varrho(r)$ along the grain axis r (perpendicular to the interface) is shown (see Figure 8c), where ϱ_A and ϱ_B are the average electron densities of lamellae A and B, respectively, $d = L_A + L_B$ is the period of the lamellar microdomain structure (i.e., the lamellar spacing), and l_A is the interface thickness of the lamellae.

In reference to Figure 8, when $\xi \gg d$ the scattering intensity $I_{obs}(q)$ from the lamellar microdomain structure is given by[38-40]

$$I_{obs}(q) \sim q^{-2} I_{theor}(q) \qquad (1)$$

where q is the magnitude of the scattering vector defined by $q = (4\pi/\lambda)\sin(\theta_z)$ (θ and λ being the

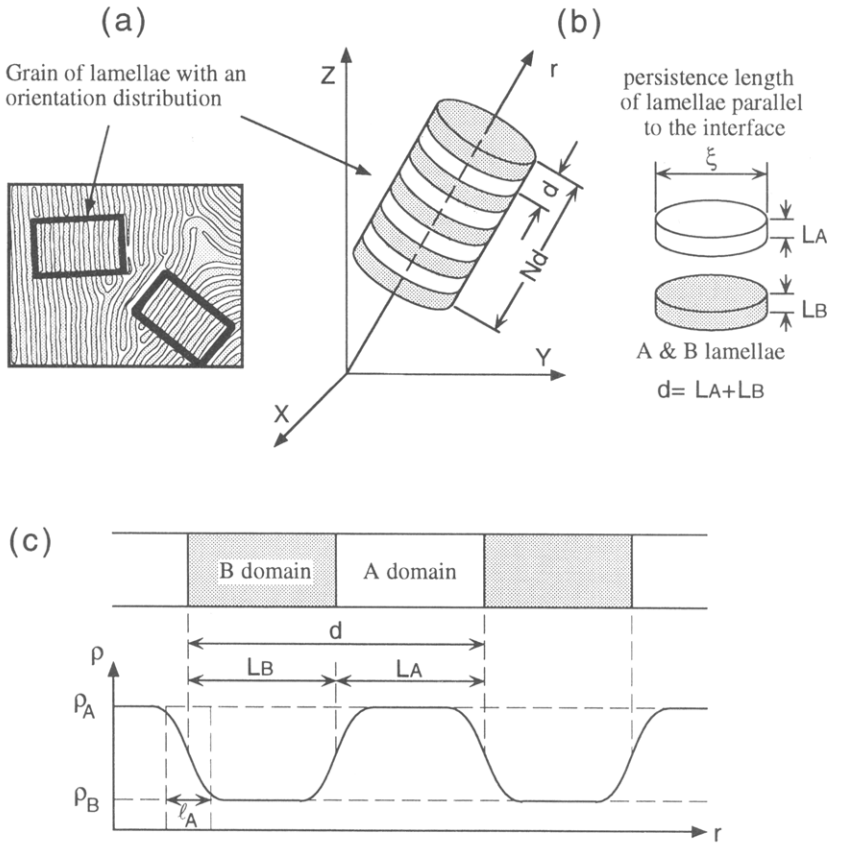

Figure 8. Schematic describing the lamellar microdomain structure: (a) an assembly of the grain units with certain orientation; (b) grain unit consisting of alternating disk-like particles with the persistence length ξ parallel to the interface; (c) electron density profile perpendicular to the interface.

scattering angle and the wavelength of the incident X-ray beam, respectively), $I_{theor}(q)$ is the scattering intensity from one grain unit along the grain axis,[37-40] and q^{-2} is the Lorentz factor related to the orientation distribution of the grain units.[38] The details about the formulation of $I_{theor}(q)$ for a lamellar system are presented elsewhere.[38,39] By fitting $I_{obs}(q)$ to the observed SAXS profiles, we can obtain the following characteristic parameters: $\bar{d}$, g, Φ_A, $\bar{L}_A$, σ_A, and σ_t, where g is the paracrystal distortion factor defined by $\Delta d/\bar{d}$ (Δd being the standard deviation of d from its average value $\bar{d}$), σ_A is the standard deviation of L_A (the thickness of lamellae A) from its average value $\bar{L}_A$, Φ_A is the volume fraction of lamellae A (i.e., $\Phi_A = \bar{L}_A/\bar{d}$), and σ_t is related to the interface thickness l_A defined $l_A = (2\pi)^{1/2}\sigma_t$. Here subscript A refers to the microdomains composed of PS and PαMS4. It should be noted that the analysis allows us to determine $\bar{d}$ and $\bar{L}_A$ independently.

The solid curves in Figure 5 denote the best-fit theoretical SAXS profiles. A good agreement was obtained between experimental and theoretical SAXS profiles. The numerical values of the characteristic parameters $\bar{d}$, g, Φ_A, $\bar{L}_A$, σ_A, and σ_t obtained by curve fitting from Figure 5 are summarized in Table 3. Uniqueness of the parameter determinations was also discussed elsewhere.[38,40]

(b) Composition Dependence. Figure 9 gives plots of Φ_A versus Φ_H, where Φ_A is the volume fraction of microdomains composed of the PS phase of K1102 and added homopolymer (PαMS4 or PS4) and Φ_H is the volume fraction of added homopolymer (PαMS4 or PS4) in the mixture. The values of Φ_A were estimated from the paracrystal analysis (see Table 3). The solid line in Figure 9 represents the situation where the entire amount of added homopolymer is assumed to be solubilized in the PS microdomains of K1102, and the PS and PB block chains are assumed to be completely segregated into the respective domains. It should be mentioned that each data point is expected to lie below the solid curve in Figure 9 either when part of the added homopolymer did not enter into the PS microdomains of K1102, thus forming *macroscopic* domains, or when part of the added homopolymer was solubilized in the PB microdomains of K1102. Therefore it is reasonable to conclude from Figure 9 that the entire amount of added homopolymer (PαMS4 or PS4) was solubilized in the PS microdomains of K1102.

Table 3. Values of the Characteristic Parameters Determined from SAXS Profiles

sample	$\bar{d}$ (nm)	g	Φ_A[a]	σ_A (nm)[a]	σ_t (nm)[b]
K1102/PαMS mixtures					
80/20	30.2	0.068	0.44	1.25	0.8
70/30	30.4	0.073	0.50	1.75	0.8
60/40	31.6	0.090	0.52	2.45	0.8
50/50	35.2	0.098	0.575	3.00	0.8
K1102/PS4 mixtures					
80/20	31.3	0.045	0.435	1.2	0.8
70/30	32.0	0.050	0.49	1.2	0.8
60/40	34.7	0.052	0.565	1.6	0.8

[a] Subscript A denotes the phase composed of the PS microdomain and added homopolymer PαMS4 or added homopolymer PS4. [b] We fixed the value of σ_t to be 0.8 nm, because this parameter has a relatively large standard deviation.[40]

Figure 10 gives plots of g-factor versus Φ_H, from which we conclude that the paracrystal distortion factor g of K1102/PS4 mixtures is much smaller than that of K1102/PαMS4 mixtures. It is of interest to note in Figure 10 that the g-factor of K1102/PαMS4 mixtures increases steadily with increasing Φ_H, while the g-factor of K1102/PS4 mixtures increases very slowly with

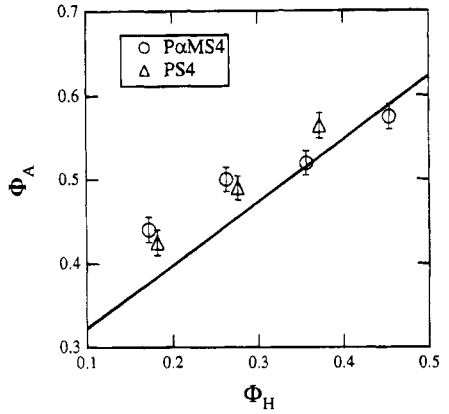

Figure 9. Plots of Φ_A versus Φ_H for K1102/PαMS4 mixtures (○) and K1102/PS4 mixtures (△), where Φ_A denotes the volume fraction of the sum of the added homopolymer (PαMS4 or PS4) and the PS block in the block copolymer K1102, Φ_H denotes the volume fraction of added homopolymer (PαMS4 or PS4), and the solid line represents the situation where the entire amount of added homopolymer (PαMS4 or PS4) was assumed to have solubilized in the PS microdomains of the block copolymer K1102 and the PB and PS block chains were assumed to be completely segregated into the respective domains.

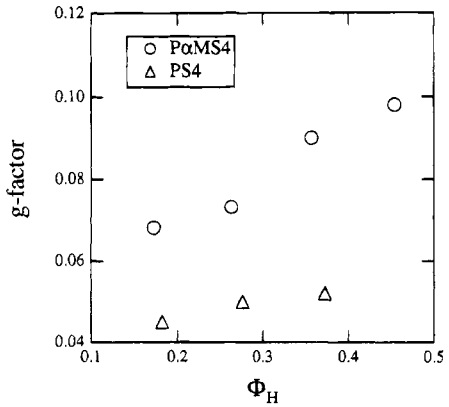

Figure 10. Plots of g-factor versus Φ_H for K1102/PαMS4 mixtures (○) and K1102/PS4 mixtures (△).

increasing Φ_H. We can conclude from this observation that the long-range order in K1102/PS4 mixtures is higher than that in K1102/PαMS4 mixtures. This suggests that added homopolymer PαMS4 was *not* distributed uniformly within the PS microdomains of K1102 and that the added PαMS4 screened the interaction between the chains of the PS block whose chemical junctions are located on the opposing interface. This screening effect increased and consequently the g-factor of K1102/PαMS4 increased as the volume fraction of added PαMS4 increased.

Figure 11 gives the normalized standard deviations $\sigma_A/\bar{L}_A$ and $\sigma_B/\bar{L}_B$ for (a) K1102/PαMS4 mixtures and (b) K1102/PS4 mixtures as a function of volume fraction of homopolymer Φ_H ($\Phi_{P\alpha MS4}$ or Φ_{PS4}), where subscript A denotes the phase composed of PS block and added homopolymer (PαMS4 or PS4) and subscript B denotes the PB block. It can be seen in Figure 11 that the values of $\sigma_A/\bar{L}_A$ and $\sigma_B/\bar{L}_B$ are smaller for the K1102/PS4 mixtures than for the K1102/PαMS4 mixtures and that the values of $\sigma_A/\bar{L}_A$ and $\sigma_B/\bar{L}_B$ for the K1102/PS4 mixtures stay more or less constant, independent of Φ_H, whereas the values of $\sigma_A/\bar{L}_A$ for the K1102/PαMS4 mixtures increase with increasing Φ_H. It is of interest to note in Figure 11 that upon increasing Φ_H, the value of $\sigma_B/\bar{L}_B$ for K1102/PαMS4 mixtures changes little, as

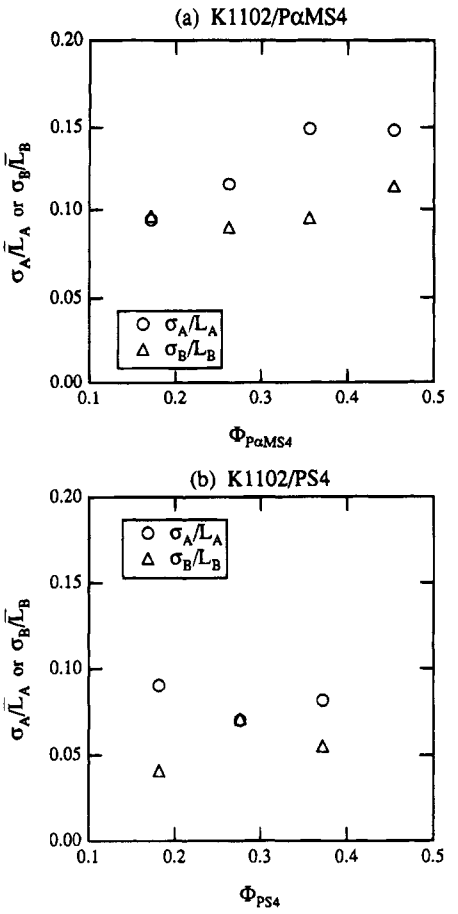

Figure 11. Plots of $\sigma_A/\bar{L}_A$ and $\sigma_B/\bar{L}_B$ for (a) K1102/PαMS4 mixtures and (b) K1102/PS4 mixtures as a function Φ_H ($\Phi_{P\alpha MS4}$ or Φ_{PS4}) of the volume fraction of added homopolymer, where the subscript A denotes the phase composed of PS block and added homopolymer (PαMS4 or PS4) and subscript B denotes the PB block phase.

compared to the value of $\sigma_A/\bar{L}_A$, implying the localized solubilization of PαMS4 in the center of the PS microdomains. Note that localized solubilization of added homopolymer does not change the average distance between chemical junctons on the interface and does not affect the regularity of the PB layer thickness. These results suggest that the thicknesses for the PB lamellae and the lamellae composed of PS block and added homopolymer are more uniform in the K1102/PS4 mixtures than in the K1102/PαMS4 mixtures. Note that large values of $\sigma_A/\bar{L}_A$ in the K1102/PαMS4 mixtures indicate *nonuniform* distribution of added homopolymer PαMS4 within the PS microdomain layer of K1102 along the interface.

In order to compare the average period of the lamellar microdoamin $\bar{d}$ and the average thickness of the PB layer $\bar{L}_B$ in K1102/PαMS4 and K1102/PS4 mixtures, respectively, paracrystal analysis was performed on the SAXS profiles measured *in situ* at 120 °C, which is higher than the glass transition temperatures of the 80/20 and 60/40 mixtures of K1102/PαMS4 and K1102/PS4. Figure 12 gives SAXS profiles of (a) K1102/PαMS4 mixtures and (b) K1102/PS4 mixtures, where the profiles with symbols denote the experimental SAXS profiles obtained at 120 °C after an annealing at this temperature (for ca. 15 min) and the curves shown with solid lines are the best-fit theoretical curves. Curve fitting was not done for the 50/50 K1102/PαMS4 mixture, because we could not observe a clear higher order peak. The numerical values of the characteristic pa-

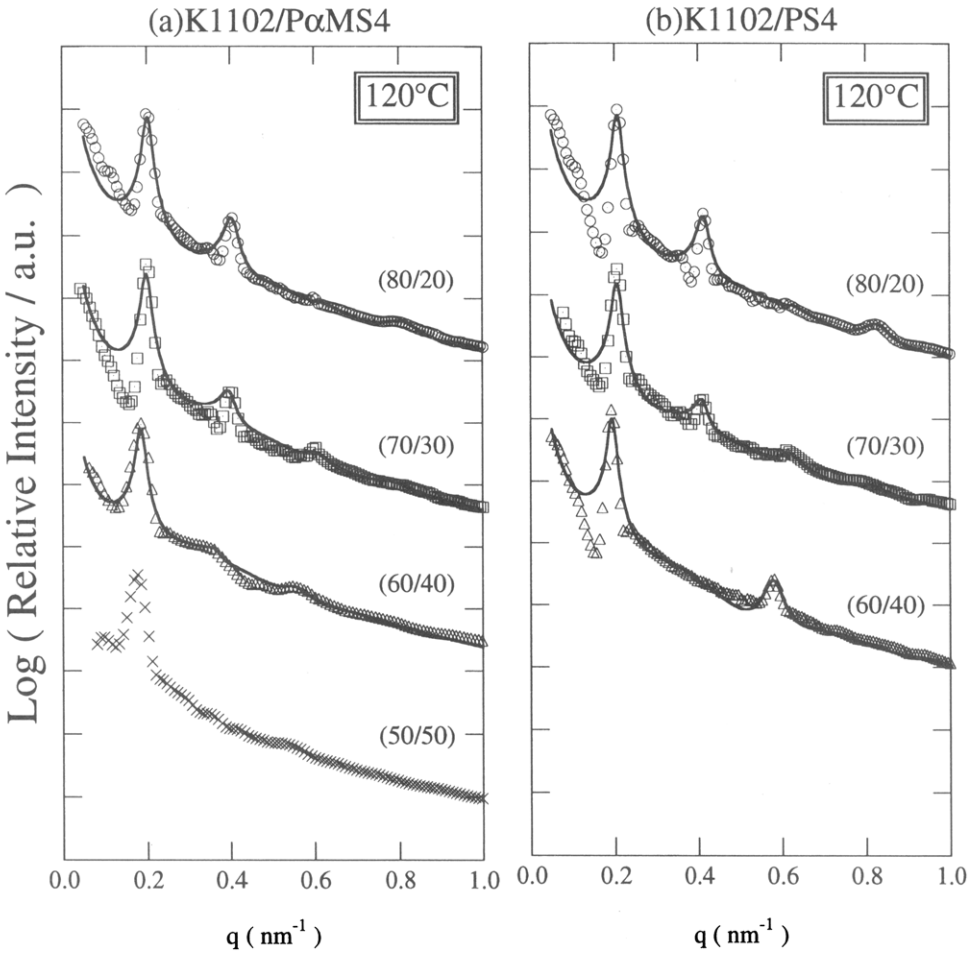

Figure 12. Plots of relative scattering intensity versus wave vector q, taken *in-situ* at 120 °C, for (a) K1102/PαMS4 mixtures and (b) K1102/PS4 mixtures, where different symbols denote different blend compositions. The solid lines denote the best-fit curves calculated using one-dimensional paracrystal theory.

Table 4. Characteristic Parameters for Calculating Best-Fit SAXS Profiles at 120 °C

sample	$\bar{d}$ (nm)	g	Φ_A[a]	σ_A (nm)[a]	σ_t (nm)[b]
K1102/PαMS mixtures					
80/20	30.9	0.065	0.38	1.4	0.8
70/30	31.4	0.070	0.43	1.7	0.8
60/40	34.0	0.079	0.49	2.2	0.8
K1102/PS4 mixtures					
80/20	30.3	0.055	0.38	1.35	0.8
70/30	30.5	0.065	0.44	1.65	0.8
60/40	32.4	0.055	0.50	1.55	0.8

[a] Subscript A denotes the phase composed of the PS microdomain and added homopolymer PαMS4 or added homopolymer PS4. [b] We fixed the value of σ_t to be 0.8 nm, because this parameter has a relatively large standard deviation.[40]

rameters obatined by curve fitting are summarized in Table 4.

Figure 13 gives (a) the average period of the lamellar microdomain structure $\bar{d}$ and (b) the average thickness of the PB layer $\bar{L}_B$ for K1102/PαMS4 mixtures and K1102/PS4 mixtures, respectively, as a function of Φ_H. It can be seen in Figure 13 that (i) the value of $\bar{d}$ increases with increasing Φ_H and the extent of increase in $\bar{d}$ is greater in K1102/PαMS4 mixtures than in K1102/PS4 mixtures, and (ii) the value of $\bar{L}_B$ decreases with increasing Φ_H and the extent of decrease in $\bar{L}_B$ is smaller in K1102/PαMS4 mixtures than in K1102/PS4 mixtures. These two results are complementary to each other, as will be described immediately. From these results we can conclude that PαMS4 tends to localize at the center of the PS microdomain of K1102 as compared to PS4 and that the change in the average distance of chemical junctiosn is smaller in K1102/PαMS4 mixtures than in K1102/PS4 mixtures. Hence, the decrease in $\bar{L}_B$ is less in K1102/PαMS4 mixtures than in K1102/PS4 mixtures. Based on the analysis presented above from the SAXS results, the spatial distribution of added homopolymer (PαMS4 or PS4) within the PS microdomains of K1102 is summarized schematically in Figure 14, which is consistent with the interpretation given above (see Figure 7) from the transmission electron micrographs.

(c) Temperature Dependence. Figure 15 gives plots of Bragg spacing $\bar{d}_B$ versus temperature for the K1102/PS4 and K1102/PαMS4 mixtures at various blend compositions. Note that $\bar{d}_B = \bar{d}$ for the lamellar microdomain. The arrow in Figure 15 indicates the T_g for each mixture and the values of T_g in Figure 15 are the same as those indicated by the vertical arrows in Figure 3. It should be mentioned that the value of T_g used for the PS phase in the mixtures of K1102/PS4 is 73 °C, which was determined from the neat K1102. This value is different from that (95 °C) reported in our previous paper,[11] which was measured with a differential scanning calorimeter. We believe that the new T_g value is more accurate than the previous one.

The Bragg spacing $\bar{d}_B$ of the K1102/PαMS4 mixtures was found to be larger than that of the K1102/PS4 mixtures at temperatures above the T_g of the mixture. This is reasonable because, as discussed above, added homopolymer PαMS4 was *not* distributed uniformly in the direction perpendicular to the lamellar interface

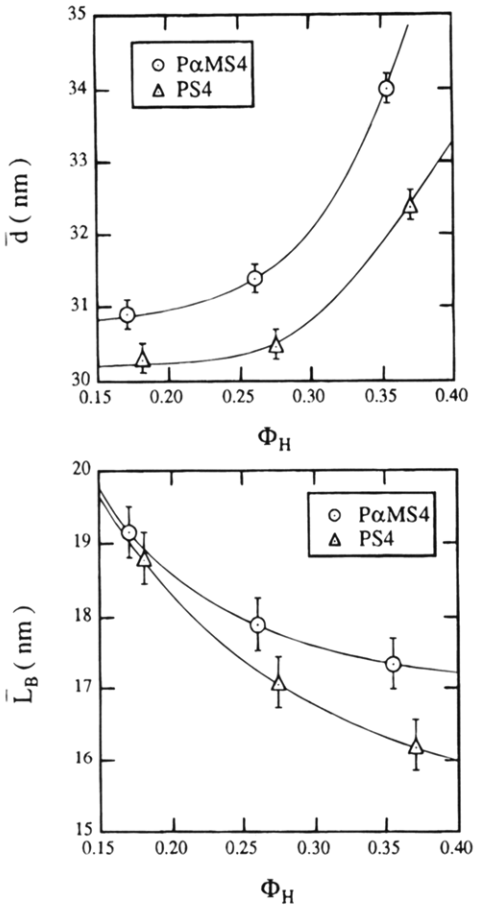

Figure 13. Plots of (a) the average interlamellar spacing $\bar{d}$ and (b) the average thickness of PB layers $\bar{L}_B$ at 120 °C versus Φ_H for K1102/PαMS4 mixtures (○) and for K1102/PS4 mixtures (△).

within the PS microdomains of K1102, as compared to added homopolymer PS4, and thus the distance between the nearest-neighbor chemical junctions of the K1102/PαMS4 mixtures was shorter than that of the K1102/PS4 mixtures. Note that the shorter the distance between the chemical junctions is, the longer the Bragg spacing $\bar{d}_B$.[1,2] Therefore the value of $\bar{d}_B$ for the K1102/PαMS4 mixtures is larger than that of the K1102/PS4 mixtures.

We found that the difference in $\bar{d}_B$ between the K1102/PαMS4 mixtures and the K1102/PS4 mixtures decreased with increasing temperature and became virtually identical at high temperatures except for the 50/50 mixtures. It should be remembered that the 50/50 K1102/PαMS4 mixture formed lamellar microdomains, while the 50/50 K1102/PS4 mixture formed cylindrical microdomains of PB in the PS matrix (see Figure 4; $\bar{d}_B \neq \bar{d}$ in this case). The temperature dependence of $\bar{d}_B$ for the lamellar microdomains was found to follow the power-law relationship

$$\bar{d}_B \sim T^{-n} \tag{2}$$

and the value of the power-law exponent n increased from about 0.4 to 1.0 as the value of Φ_H increased from 0.2 to 0.5. However, we found that all the data tend to deviate from the power-law behavior at higher temperatures, as reported in our previous paper,[3] which we believe reflects the order−disorder transition occurring at those high temperatures.

Figure 16 gives a schematic describing the change of microdomain structure with temperature. At low temperature (see Figure 16a), added PαMS4 is *not* uniformly distributed within the microdomains of K1102 in the direction both perpendicular and parallel to the interface. As the temperature increases, the repulsive interaction between the PS chains and the PαMS4 chains decreases and thus the contribution of the contact energy E_{domain} to free energy decreases. As a result, as the temperature is increased, the added homopolymer PαMS4 tends to be more uniformly distributed within the PS microdomains of K1102, and concentration fluctuations of PαMS4 in the direction both perpendicular and parallel to the interface tend to decrease (see Figure 16b).

As added homopolymer PαMS4 becomes distributed more uniformly within the PS microdomains of K1102,

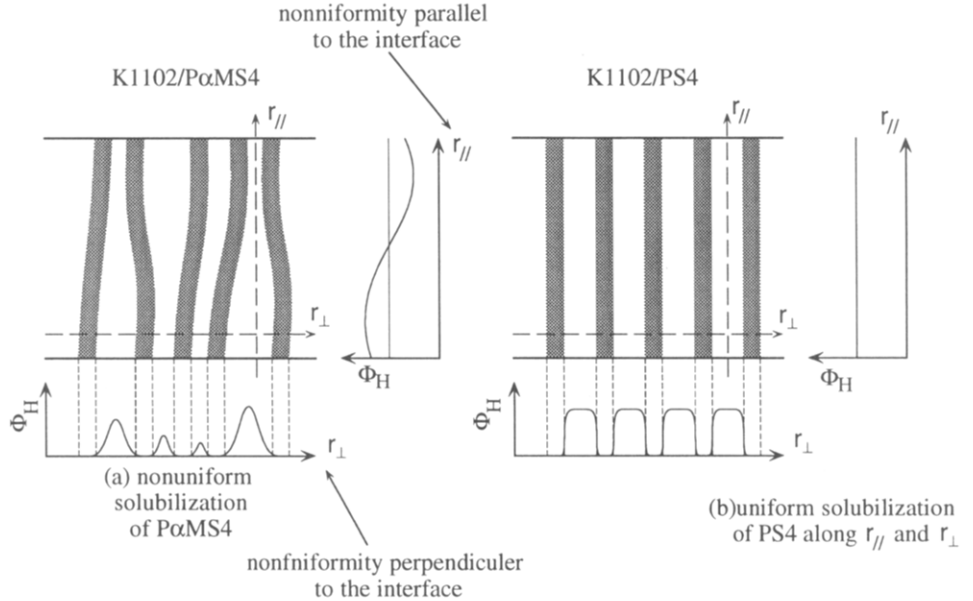

Figure 14. Schematic describing the spatial distribution of added homopolymer Φ_H within the PS microdomains of the block copolymer K1102: (a) nonuniform distribution of added PαMS4 (note that nonuniformity occurs in the direction parallel ($r_{||}$) and perpendicular to the lamellar interface ($r_\perp$)) as shown in $\Phi_H(r_{||}, r_\perp)$ and (b) uniform distribution of added PS4 as shown again in $\Phi_H(r_{||}, r_\perp)$. Φ_H designates the volume fraction of PαMS4 or PS4 in the PS microdomains. The dark and bright phases correspond to the PB microdomains and the microdomains composed of PS and PαMS4 or PS4, respectively.

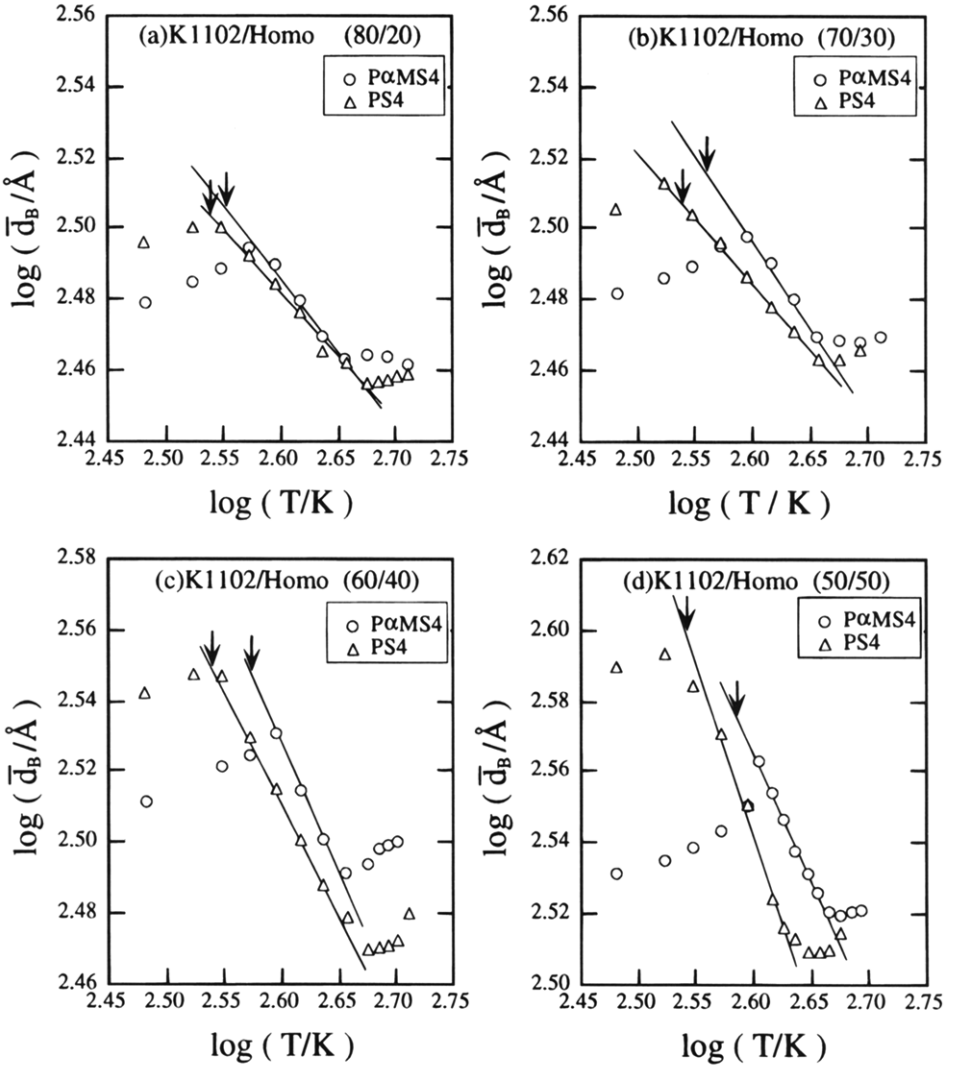

Figure 15. Plots of Bragg spacing $\bar{d}_B$ versus temperature for (a) 80/20 K1102/PαMS4 (○) and 80/20 K1102/PS4 (△), (b) 70/30 K1102/PαMS4 (○) and 70/30 K1102/PS4 (△), (c) 60/40 K1102/PαMS4 (○) and 60/40 K1102/PS4 (△), and (d) 50/50 K1102/PαMS4 (○) and 50/50 K1102/PS4 (△).

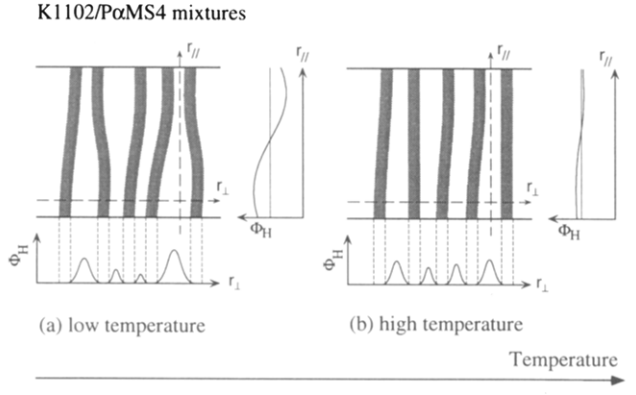

Figure 16. Schematic describing the spatial distribution of added PαMS4 within the PS microdomains of the block copolymer K1102: (a) at low temperature and (b) at high temperature. $\Phi_H(r_{\parallel},r_{\perp})$ and bright and dark microphases have the same meaning as those in Figure 14.

the distance between nearest-neighbor chemical junctions a_J increases, and thus the value of Bragg spacing $\bar{d}_B$ decreases. This may be the reason why the value of n appearing in eq 2 is larger for the K1102/PαMS4 mixtures than for the K1102/PS4 mixtures. The extent of the contribution of E_{domain} to the free energy is expected to increase with increasing Φ_H, and thus the contact energy E_{domain} becomes less with increasing temperature and, also, with increasing Φ_H. As a result, the value of n increases with increasing Φ_H.

It should be mentioned that blends of PS and PαMS exhibit an upper critical solution temperature[41,42] and hence the miscibility between the two components increases with increasing temperature. Therefore, the experimental observation made above that added homopolymer PαMS4 is distributed more uniformly within the PS microdomains of K1102 with increasing temperature is attributable to an enhanced miscibility between PαMS and PS.

V. Concluding Remarks

The spatial distribution of added homopolymers PS and PαMS within the PS microdomains of an SBS triblock copolymer (Kraton 1102) was investigated using SAXS and TEM. The SAXS profiles obtained were analyzed using one-dimensional paracrystal theory. It was found that each of the added homopolymers, PS and PαMS, was solubilized into the PS microdomains of Kraton 1102, but the spatial distribution was different in the two cases. Specifically, added homopolymer PαMS tends to be solubilized nonuniformly in the PS microdomain of Kraton 1102 in the directions both parallel and perpendicular to the interface, while added

homopolymer PS tends to be unformly solubilized in the PS microdomains of Kraton 1102. The localized, nonuniform solubilization of PαMS developed regions which were either rich or poor in PαMS within the PS microdomain and deformed the interface, which made the regularity of microdomains low. The localized, nonuniform solubilization of PαMS is induced by the repulsive interaction between PαMS and PS. Added homopolymer PαMS tends to be solubilized more uniformly in the PS microdomain of Kraton 1102 with increasing temperature, since the repulsive interaction decreases with increasing temperature.

References and Notes

(1) Hashimoto, T.; Tanaka, H.; Hasegawa, H. *Macromolecules* **1990**, *23*, 4378.
(2) Tanaka, H.; Hasegawa, H.; Hashimoto, T. *Macromolecules* **1991**, *24*, 240.
(3) Tanaka, H.; Hashimoto, T. *Macromolecules* **1991**, *24*, 5713.
(4) Hashimoto, T.; Koizumi, S.; Hasegawa, H; Izumitani, T.; Hyde, S. T. *Macromolecules* **1992**, *25*, 1433.
(5) Winey, K. I.; Thomas, E. L.; Fetters, L. J. *J. Chem. Phys.* **1991**, *95*, 9367.
(6) Winey, K. I.; Thomas, E. L.; Fetters, L. J. *Macromolecules* **1992**, *25*, 422; **1992**, *25*, 2645.
(7) Spontak, R. J.; Smith, S. D.; Ashraf, A. *Macromolecules* **1993**, *26*, 956; **1993**, *26*, 5118.
(8) Disko, M. M.; Liang, K. S.; Behal, S. K.; Roe, R. J.; Jean, K. J. *Macromolecules* **1993**, *26*, 2983.
(9) Jeon, K. J.; Roe, R. J. *Macromolecules* **1994**, *27*, 2439.
(10) Löwenhaupt, B.; Steurer, A.; Hellmann, G. P.; Gallot, Y. *Macromolecules* **1994**, *27*, 908.
(11) Han, C. D.; Baek, D. M.; Kim, J.; Kimishima, K.; Hashimoto, T. *Macromolecules* **1992**, *25*, 3052.
(12) Hashimoto, T.; Kimishima, K.; Hasegawa, H. *Macromolecules* **1991**, *24*, 5704.
(13) Hashimoto, T.; Izumitani, T.; Oono, K. *Makromol. Chem., Macromol. Symp.*, in press.
(14) Kim, J. K.; Jung, D. S.; Kim, J. *Polymer* **1993**, *34*, 4613.
(15) Roe, R. J.; Zin, W. C. *Macromolecules* **1984**, *17*, 189.
(16) Baek, D. M.; Han, C. D.; Kim, J. K. *Polymer* **1992**, *33*, 4821.
(17) Zin, W. C.; Roe, R. J. *Macromolecules* **1984**, *17*, 183.
(18) Nojima, S.; Roe, R. J. *Macromolecules* **1987**, *20*, 1866.
(19) Owens, J. N.; Gancarz, I. S.; Koberstein, J. T.; Russell, T. P. *Macromolecules* **1989**, *22*, 3388.
(20) Mori, K.; Tanaka, H.; Hashimoto, T. *Macromolecules* **1987**, *20*, 381.
(21) Tanaka, H.; Hashimoto, T. *Polym. Commun.* **1988**, *29*, 212.
(22) Leibler, L. *Macromolecules* **1980**, *13*, 1602.
(23) Kim, J. K.; Kimishima, K.; Hashimoto, T. *Macromolecules* **1993**, *26*, 125.
(24) Hong, K. M.; Noolandi, J. *Macromolecules* **1983**, *16*, 1083.
(25) Whitmore, M. D.; Noolandi, J. *Macromolecules* **1985**, *18*, 2486.
(26) Koizumi, S.; Hasegawa, H.; Hashimoto, T. Makromol. *Chem. Macromol. Symp.* **1992**, *62*, 1992.
(27) Hashimoto, T.; Tanaka, H.; Hasegawa, H. In *Molecular Conformation and Dynamics of Macromolecules in Condensed Systems*; Nagasawa, M., Ed.; Elsevier Amsterdam, 1988; p 257.
(28) Koizumi, S.; Hasegawa, H.; Hashimoto, T. *Macromolecules* **1994**, *27*, 7893.
(29) Mayes, A. M.; Russell, T. P.; Satija, S. K.; Majkrazak, C. F. *Macromolecules* **1992**, *25*, 6523.
(30) Shull, K. R.; Winey, K. I. *Macromolecules* **1992**, *25*, 2637.
(31) Hadziioannou, G.; Picot, C.; Skoulios, A.; Ionescu, M. L.; Mathis, A.; Duplessix, R.; Gallot, Y.; Lingelser, J. P. *Macromolecules* **1982**, *15*, 263.
(32) Hasegawa, H.; Hashimoto, T.; Kawai, H.; Lodge, T. P.; Amis, E. J.; Glinka, C. J.; Han, C. C. *Macromolecules* **1985**, *18*, 67.
(33) Hasegawa, H.; Tanaka, H.; Hashimoto, T.; Han, C. C. *Macromolecules* **1987**, *20*, 2120.
(34) Hasegawa, H.; Tanaka, H.; Hashimoto, T.; Han, C. C. *J. Appl. Crystallogr.* **1991**, *24*, 672.
(35) Richardson, M. J.; Saville, N. G. *Polymer* **1977**, *18*, 3.
(36) Cowie, J. M. G.; Toporowski, P. M. *J. Macromol. Sci., Phys.* **1969**, *B3*, 81.
(37) Hashimoto, T.; Nagatoshi, K.; Todo, A.; Hasegawa, H.; Kawai, H. *Macromolecules* **1974**, *7*, 364.
(38) Shibayama, M.; Hashimoto, T. *Macromolecules* **1986**, *19*, 740.
(39) Sakurai, S.; Okamoto, S.; Kawamura, T.; Hashimoto, T. *J. Appl. Crystallogr.* **1991**, *24*, 679.
(40) Hashimoto, T.; Kawamura, T.; Harada, M.; Tanaka, H. *Macromolecules* **1994**, *27*, 3063.
(41) Lin, J. L.; Roe, R. J. *Polymer* **1988**, *29*, 127.
(42) Han, C. D., in preparation.

MA946172W